

# Atomic Trajectory Modeling with State Space Models for Biomolecular Dynamics

Liang Shi<sup>1,2</sup> Jiarui Lu<sup>3,4</sup> Junqi Liu<sup>1,2</sup> Chence Shi<sup>2</sup> Zhi Yang<sup>1</sup> Jian Tang<sup>2,3,5,6</sup>

## Abstract

Understanding the dynamic behavior of biomolecules is fundamental to elucidating biological function and facilitating drug discovery. While Molecular Dynamics (MD) simulations provide a rigorous physical basis for studying these dynamics, they remain computationally expensive for long timescales. Conversely, recent deep generative models accelerate conformation generation but are typically either failing to model temporal relationship or built only for monomeric proteins. To bridge this gap, we introduce ATMOS, a novel generative framework based on State Space Models (SSM) designed to generate atom-level MD trajectories for biomolecular systems. ATMOS integrates a Pairformer-based state transition mechanism to capture long-range temporal dependencies, with a diffusion-based module to decode trajectory frames in an autoregressive manner. ATMOS is trained across crystal structures from PDB and conformation trajectory from large-scale MD simulation datasets including mdCATH and MISATO. We demonstrate that ATMOS achieves state-of-the-art performance in generating conformation trajectories for both protein monomers and complex protein-ligand systems. By enabling efficient inference of atomic trajectory of motions, this work establishes a promising foundation for modeling biomolecular dynamics.

## 1. Introduction

Elucidating the functional mechanisms of biomolecules requires a comprehensive understanding of protein dynamics, rather than merely analyzing static crystal structures. Traditionally, Molecular Dynamics (MD) simulations are the

gold standard for this task, relying on fundamental physical principles to reveal critical thermodynamic and kinetic properties. However, despite rigorous adherence to physical laws, traditional MD methods are computationally expensive, often struggling to access biologically relevant timescales or sample rare conformational transitions efficiently.

To alleviate these computational burdens, recent research has pivoted toward deep generative models. Broadly, these approaches fall into two categories. The first focuses on ensemble generation, where models like AlphaFlow (Jing et al., 2024a) and BioEmu (Lewis et al., 2025) emulate the equilibrium Boltzmann distribution. However, they typically generate samples in an independent and identically distributed (*i.i.d.*) manner, and fail to reveal kinetic pathways by discarding temporal correlations. The second category attempts generative trajectory modeling, represented by recent works such as MDGen (Jing et al., 2024b), ConfRover (Shen et al., 2025), and TEMPO (Xu et al., 2025b). While these methods begin to take the time dimension into consideration, they cannot model complex systems of biomolecules.

Addressing the aforementioned limitation, we introduce Atomic Trajectory **MO**deling with **SSM**s (**ATMOS**), which formulates biomolecular dynamics generation as a sequence modeling problem. ATMOS leverages State Space Models (SSM) to efficiently capture long-horizon trajectory evolution with linear computational complexity in terms of the trajectory length. To ensure geometric modeling capacity during temporal propagation, we parameterize the SSM state transition function using an adapted Pairformer module (Abramson et al., 2024), effectively modeling geometric interactions within the latent evolution. Critically, unlike previous practices, this framework operates on an atom-level coordinate representation by encoding states and decoding predicted trajectories without coarse-graining, thereby preserving detailed geometric contexts. The training data of ATMOS comprises static structural data from the Protein Data Bank (PDB) and large-scale MD simulation data from mdCATH (Mirarchi et al., 2024) and MISATO (Siebenmorgen et al., 2024). Experimental results demonstrate that the proposed ATMOS effectively models high-quality biomolecular dynamics, achieving state-of-the-art performance in generating conformation trajectories on both protein monomer and

<sup>1</sup>School of Computer Science, Peking University <sup>2</sup>BioGeometry  
<sup>3</sup>Mila - Québec AI Institute <sup>4</sup>Université de Montréal <sup>5</sup>HEC  
Montréal <sup>6</sup>CIFAR AI Chair. Correspondence to: Zhi Yang  
<yangzhi@pku.edu.cn>, Jian Tang <jian.tang@hec.ca>.

protein-ligand benchmarks. Our contributions to the field are summarized as follows:

- We present a unified generative framework for simulating dynamics of biomolecules, generalizing from monomeric proteins to complex biomolecular systems.
- ATMOS models dynamics at the fully atomic level by operating directly on atomic coordinates during both the encoding and decoding phases, rather than coarse-graining representations like  $C\alpha$  atoms or backbone frames.
- We innovatively adapt State Space Models to the trajectory generation, enabling the capture of long-range temporal dependencies with improved inference efficiency compared to traditional simulation or purely attention-based approaches.
- ATMOS demonstrates SOTA performance in generating trajectories on large-scale MD datasets, specifically mdCATH and MISATO, validating the model’s ability to generalize across diverse biological systems.
- By successfully bridging static structural priors with dynamic trajectory generation, ATMOS extends the static structure prediction into the dynamics domain, paving the way towards dynamics foundation models.

## 2. Related Work

**Generative Modeling of Protein Ensembles.** Early data-driven approaches for exploring protein conformational landscapes focused on modifying inputs to high-accuracy single-structure predictors. Methods such as MSA subsampling (Del Alamo et al., 2022; Wayment-Steele et al., 2024) perturb the multiple sequence alignment fed into AlphaFold2 to reveal alternative states, though these inference-time interventions often lack conformation diversity (Jing et al., 2024a). To directly model equilibrium distributions, deep generative models have been developed to sample conformations *i.i.d.*. Seminal work such as Boltzmann Generators (Noé et al., 2019) utilized normalizing flows to sample from the Boltzmann distribution, though scaling to systems beyond training remained challenging. Recent advances leverage diffusion and flow matching on large-scale MD datasets; for instance, AlphaFlow (Jing et al., 2024a) fine-tunes pre-trained folding models to capture ensemble diversity, while EBA (Lu et al., 2025a) enhances this framework with physical energy-based alignment. Other approaches focus on specific physical constraints or data regimes: Distributional Graphormer (DiG) (Zheng et al., 2024) and ConfDiff (Wang et al., 2024) incorporate energy or force guidance to improve physical validity, Str2Str (Lu et al., 2024a) employs a zero-shot translation framework

without reliance on MD training data, ESMDiff (Lu et al., 2025b) adopts latent language modeling to efficiently sample conformation ensembles, and BioEmu (Lewis et al., 2025) integrates experimental stability data to predict thermodynamic properties.

**Generative Modeling of Molecular Trajectories.** While ensemble models capture time-independent distributions, trajectory generation methods aim to emulate the temporal evolution of molecular systems, serving as surrogates for expensive Molecular Dynamics (MD) simulations. Initial efforts, such as ITO (Schreiner et al., 2023), TimeWarp (Klein et al., 2023) and EquiJump (Costa et al., 2024), focused on learning time-coarsened transition operators to jump over large time steps. More recent frameworks model the joint distribution of entire trajectories to capture long-range temporal dependencies. MDGen (Jing et al., 2024b) treats trajectories as time-series of 3D structures, utilizing flow matching to enable forward simulation, transition path interpolation, and upsampling. To handle the multi-scale nature of protein motions, TEMPO (Xu et al., 2025b) introduces a hierarchical trajectory generation framework that separates slow collective motions from fast local fluctuations. Similarly, ConfRover (Shen et al., 2025) employs a causal transformer with an SE(3) diffusion decoder to simultaneously learn conformational distributions and dynamics. Other specialized architectures include BioMD (Feng et al., 2025) for protein-ligand unbinding pathways, and PTraj-Diff (Xu et al., 2025a) for protein-protein complex dynamics.

## 3. Method

### 3.1. Preliminaries

**Problem Formulation.** We conceptualize the generation of biomolecular trajectory as a conditional sequence modeling task. Consider a biomolecular system consisting of  $N$  atoms. We represent the dynamic evolution of this system as a trajectory of coordinates  $\mathbf{X} = (\mathbf{x}_1, \mathbf{x}_2, \dots, \mathbf{x}_T) \in \mathbb{R}^{T \times N \times 3}$ , where  $\mathbf{x}_t \in \mathbb{R}^{N \times 3}$  denotes the 3D Cartesian coordinates of all  $N$  atoms at time step  $t$ , and  $T$  represents the trajectory length, i.e., the number of frames. In addition to coordinates, the system is defined by time-invariant atomic features  $\mathbf{a}$ , where  $\mathbf{a} \in \mathbb{R}^{N \times d_a}$  represents atom-level attributes including atom type, residue type, molecule-level identifiers that indicate whether an atom belongs to a protein or ligand, etc.

Our objective is to learn a generative model  $p_\theta$  that approximates the true distribution of trajectories given the initial conformation  $\mathbf{x}_1$  and the context  $\mathbf{a}$ . Following standard autoregressive practices, we factorize the joint probability over the temporal dimension:

$$p_\theta(\mathbf{X}|\mathbf{x}_1, \mathbf{a}) = \prod_{t=1}^{T-1} p_\theta(\mathbf{x}_{t+1}|\mathbf{x}_{1:t}, \mathbf{a}) \quad (1)$$

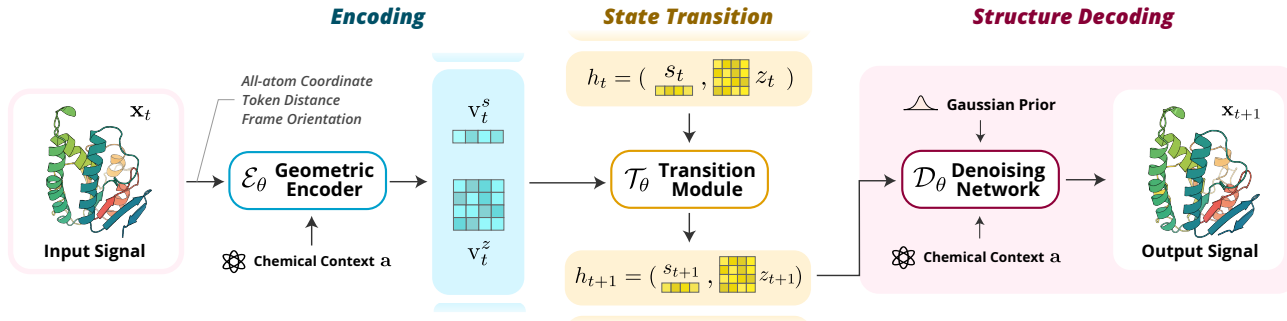


Figure 1. Overview of the Proposed Atomic Trajectory Modeling Framework.

This formulation allows the model to generate physically consistent long-horizon dynamics by conditioning the next state on the history of the trajectory and the chemical identity of the system.

**State Space Models (SSM).** State Space Models (Gu et al., 2021a;b) provide a unified framework for modeling sequential data by mapping a 1-dimensional input signal  $u(t) \in \mathbb{R}$  to an output signal  $y(t) \in \mathbb{R}$  through a latent state  $h(t) \in \mathbb{R}^D$ . In their continuous-time form, linear SSMs are defined by the following ordinary differential equations (ODEs):

$$\dot{h}(t) = \mathbf{A}h(t) + \mathbf{B}u(t), \quad y(t) = \mathbf{C}h(t) \quad (2)$$

where  $\mathbf{A} \in \mathbb{R}^{D \times D}$ ,  $\mathbf{B} \in \mathbb{R}^{D \times 1}$ , and  $\mathbf{C} \in \mathbb{R}^{1 \times D}$  are learnable projection matrices. To apply this framework to discrete sequence data (such as MD trajectories sampled at fixed intervals  $\Delta$ ), the continuous system is discretized—typically via the Zero-Order Hold (ZOH) method—yielding the recurrence:

$$h_t = \bar{\mathbf{A}}h_{t-1} + \bar{\mathbf{B}}u_t, \quad y_t = \mathbf{C}h_t \quad (3)$$

Here,  $\bar{\mathbf{A}}$  and  $\bar{\mathbf{B}}$  are the discretized state parameters. This recurrent formulation allows for efficient  $O(1)$  inference per step, making SSM particularly well-suited for generating long molecular trajectories compared to the quadratic complexity of standard attention mechanisms.

**Notations.** Throughout this paper, we use bold lowercase letters (e.g.,  $\mathbf{x}$ ,  $\mathbf{h}$ ) for vectors and atom-level representations, and bold or calligraphic uppercase letters (e.g.,  $\mathbf{A}$ ,  $\Phi$ ,  $\mathcal{E}$ ) for matrices and operations. We denote the coordinate of the  $i$ -th atom at time  $t$  as  $\mathbf{x}_{t,i} \in \mathbb{R}^3$ . The set of all atoms is indexed by  $i \in \{1, \dots, N\}$ , and discrete time steps are indexed by  $t \in \{1, \dots, T\}$ .

### 3.2. An Atomic Trajectory Modeling Framework

**SSM as Learnable Biomolecular Simulators.** We frame the generation of biomolecular trajectories as the learning of a time-continuous evolution function, functionally analogous to the integrator used in classical MD simulations. In

traditional MD simulations, the system evolves according to an integrator that explicitly calculates future positions based on current coordinates, momenta, and inter-atomic forces derived from a force field. While rigorous, this process is computationally intensive for long timescales.

To overcome this, ATMOS adopts SSM as efficient, learnable biomolecular propagators. Unlike standard attention-based sequence models that must revisit the entire history for every prediction, SSM maintains a latent recurrent state. This aligns with the physical reality of molecular dynamics, which is inherently Markovian: the future evolution of a system is governed by its current *phase-space* state (positions and momenta) rather than its explicit history. By replacing the expensive numerical integrator with a neural SSM, we achieve a framework that is both physically intuitive and computationally efficient for long-horizon generation.

**Specifications.** Formally, we instantiate the SSM framework for atomic trajectory modeling by defining the input signal, latent state, and output prediction as follows:

- **Input Signal ( $\mathbf{x}_t$ ):** The time-varying input to the model is the configuration of the system at time  $t$ , represented by the atomic coordinates  $\mathbf{x}_t \in \mathbb{R}^{N \times 3}$ . This serves as the observable states of the sequence.
- **Latent State ( $\mathbf{h}_t$ ):** The recurrent hidden state  $\mathbf{h}_t$  acts as an implicit representation of the system’s complete phase-space state. While the input  $\mathbf{x}_t$  provides only the geometric configuration, the latent state  $\mathbf{h}_t$  captures the auxiliary dynamic variables necessary for propagation. Intuitively,  $\mathbf{h}$  effectively encodes implicit momenta, acting forces, and the thermodynamic memory (e.g., thermostat states) required to govern the Langevin dynamics of the system.
- **Output Signal ( $\mathbf{x}_{t+1}$ ):** Conditioning on the updated latent  $\mathbf{h}_{t+1}$ , the model operates autoregressively to predict the updated coordinates  $\mathbf{x}_{t+1} \in \mathbb{R}^{N \times 3}$  for the subsequent time step.

**Learning Objective.** This framework provides two crit-

ical advantages. First, the constant inference complexity of SSMs per step (in recurrent mode) allows ATMOS to generate trajectories of arbitrary length  $T$  with linear scaling, addressing the bottleneck of existing autoregressive methods. Second, the continuous-time formulation of SSMs naturally handles the temporal correlations inherent in physical motion, smoothing the modeling of rare conformational transitions. Under this framework, ATMOS can be trained to maximize the likelihood of the ground-truth trajectory  $\mathbf{X}$  given the chemical context  $\mathbf{a}$ . The learning objective is:

$$\mathcal{L}_{\text{SSM}} = - \sum_{t=1}^{T-1} \log p_{\theta}(\mathbf{x}_{t+1} | \mathbf{h}_t, \mathbf{x}_t, \mathbf{a}) \quad (4)$$

where  $p_{\theta}$  is parameterized by the predicted shift in coordinates.

### 3.3. Model Architecture

**Compact Coupled Latent Representation.** While our framework operates on full atomic coordinates to ensure precise dynamics, modeling interactions at the all-atom scale for large biomolecular systems is computationally prohibitive. To reconcile resolution with efficiency, we adopt a compact (partially coarse-grained) *coupled latent* widely used in modern structure prediction architectures (Jumper et al., 2021; Abramson et al., 2024). Specifically, we define the latent SSM state  $\mathbf{h}_t$  as a coupled representation operating on a tokenized sequence of length  $L$  (where  $L \leq N$ ):

$$\mathbf{h}_t \triangleq (\mathbf{s}_t, \mathbf{z}_t). \quad (5)$$

Here, the system is tokenized such that atom-level representations of protein are grouped into residue-level latents, otherwise the atomic resolution is retained. Consequently,  $\mathbf{s}_t \in \mathbb{R}^{L \times d_s}$  denotes the *single representation*, capturing the state of each residue or ligand atom, and  $\mathbf{z}_t \in \mathbb{R}^{L \times L \times d_z}$  denotes the *pair representation*, encoding the interactions between tokens. This coupled representation allows ATMOS to efficiently model long-range dependencies within the computationally manageable latent space, while keeping the observable state as fine-grained atomic coordinates ( $N$ ).

**Neural SSM Parametrization.** While classical SSMs rely on linear projections (Eq. 2), modeling complex molecular interactions requires high-capacity non-linear transitions. Based on the coupled latent space, one can effectively parameterize the state evolution using neural networks. The architecture is composed of three functional modules:

*Context and Input Encoding.* We first initialize the latent state by tokenizing the chemical context  $\mathbf{a}$ . An embedding layer maps contexts such as atom types and residue indices to the initial state  $\mathbf{h}_0 \triangleq (\mathbf{s}_0, \mathbf{z}_0) = \mathbf{e}_{\theta}(\mathbf{a})$ , establishing the context prior of the system before dynamics begin. At each time step  $t$ , the input signal  $\mathbf{x}_t$  (current atomic coordinates)

must be injected into the latent space to update the system’s trajectory. We employ a geometric encoder  $\mathcal{E}_{\theta}$  to extract features from  $\mathbf{x}_t$  and fuses them with the static attributes  $\mathbf{a}$ :

$$\mathbf{v}_t = (\mathbf{v}_t^s, \mathbf{v}_t^z) = \mathcal{E}_{\theta}(\mathbf{x}_t, \mathbf{a}) \quad (6)$$

This term  $\mathbf{v}_t$  acts as the forcing term<sup>1</sup> (analogous to  $\mathbf{B}\mathbf{u}_t$  in Eq. 3), representing the instantaneous geometric update derived from the current frame  $\mathbf{x}_t$ .

*State Transition.* The core propagator of ATMOS is the state transition function  $\mathcal{T}_{\theta}$ , which evolves the latent state  $\mathbf{h}$  from  $t$  to  $t + 1$ . We instantiate this transition using a variant of the Pairformer module (Abramson et al., 2024), denoted as  $\Phi_{\theta} : \mathbf{s}, \mathbf{z} \mapsto \mathbf{s}', \mathbf{z}' \in \mathbb{R}^{L \times d_s}, \mathbb{R}^{L \times L \times d_z}$ . The Pairformer is uniquely suited for this role as it enables bidirectional information flow between the single and pair tracks (Algorithm 2). The discretized update rule is defined as ( $\Delta t > 0$  indicates the time step):

$$\mathbf{h}_{t+1} \triangleq (\mathbf{s}_{t+1}, \mathbf{z}_{t+1}) = \mathcal{T}_{\theta}(\mathbf{h}_t, \mathbf{v}_t, \Delta t). \quad (7)$$

Here, the transition kernel  $\mathcal{T}_{\theta}$  is defined as

$$\begin{aligned} \mathcal{T}_{\theta}(\mathbf{h}_t, \mathbf{v}_t, \Delta t) &\triangleq \mathcal{T}_{\theta}(\mathbf{s}_t, \mathbf{z}_t; \mathbf{v}_t^s, \mathbf{v}_t^z; \Delta t) = \\ &\Phi_{\theta}(\mathbf{s}_t + \mathbf{v}_t^s + \tau_{\theta}(\Delta t), \mathbf{z}_t + \mathbf{v}_t^z + \tau_{\theta}(\Delta t)), \end{aligned} \quad (8)$$

where  $\tau_{\theta}(\cdot)$  is broadcasted learnable timestep embeddings. Intuitively, the Pairformer  $\Phi_{\theta}$  functions as a learnable integrator, calculating the next latent state by reasoning over the previous memory  $\mathbf{h}_t$  and the current geometric update  $\mathbf{v}_t$ .

*Structure Decoding.* Finally, to map the evolved latent state back to the coordinate space, we employ a diffusion-based decoder. We model the generation of the next frame  $\mathbf{x}_{t+1}$  as a reverse diffusion process. The core component is a denoising network  $\mathcal{D}_{\theta}$  that predicts the clean, denoised structure from a noisy state. Specifically, for a given trajectory step  $t + 1$ , we introduce a diffusion time variable  $\gamma \in [0, +\infty]$  to distinguish the diffusion time from the trajectory index  $t$ . The decoder is conditioned on the noisy structure  $\tilde{\mathbf{x}}^{(\gamma)}$ , the chemical context  $\mathbf{a}$ , and the evolved latent representations ( $\mathbf{h}_{t+1}$ ). The denoising operation is defined as:

$$\hat{\mathbf{x}}_{t+1} = \mathcal{D}_{\theta}(\tilde{\mathbf{x}}^{(\gamma)}, \mathbf{a}, \mathbf{h}_{t+1}, \gamma) \quad (9)$$

where  $\hat{\mathbf{x}}_{t+1}$  represents the predicted denoised coordinates. By conditioning on the dual latent state ( $\mathbf{s}_{t+1}, \mathbf{z}_{t+1}$ ), the diffusion model is guided by both the detailed atomic state and the pairwise geometric constraints, ensuring the generated structures are both chemically valid and dynamically consistent with the trajectory history.

<sup>1</sup>Note that variables  $\mathbf{v}_t^s \in \mathbb{R}^{L \times d_s}$  and  $\mathbf{v}_t^z \in \mathbb{R}^{L \times L \times d_z}$  are defined on the tokenized space and scale with the length  $L$ , whereas  $\mathbf{x}_t \in \mathbb{R}^{N \times 3}$  is defined in the raw coordinate space.

### 3.4. Training Objectives

**Training Regime.** To efficiently train ATMOS on long-horizon MD trajectory data, we employ a teacher-forcing (Williams & Zipser, 1989) with subsampling strategy during the training stage. Rather than unrolling the full trajectory, we optimize the model on sub-trajectory windows and input the prefix states as the ground truth. Specifically, for a given training trajectory  $\mathbf{X} = (\mathbf{x}_1, \dots, \mathbf{x}_T)$  of length  $T$ , we sample a start index  $t_0$ , a temporal stride  $\Delta t$ , and a window size  $k$  such that  $1 \leq t_0 < t_0 + k\Delta t \leq T$ . The model processes the first  $k - 1$  frames as context to predict the target state  $\mathbf{x}_{t_0+k\Delta t}$  at the strided  $k$ -th step. For simplicity, we adopt a fixed stride in this work, whereas we believe it is worth exploring learn dynamics across varied timescales by randomizing  $\Delta t$ .

**Loss Functions.** As the learning objective, we train ATMOS end-to-end with two important loss terms: (1) latent fidelity loss (distogram) and (2) reconstruction loss (diffusion), which are detailed as follows.

*Latent Fidelity Loss (Distogram).* To enforce geometric consistency in the latent space, we impose a distogram-based latent fidelity loss. Following Abramson et al. (2024), a lightweight prediction head  $\mathbf{P}_\theta$  is applied to the pair representation  $\mathbf{z}_t$ , which outputs a 64-bin probability distribution over discretized distances for each token pair  $(i, j)$ . The distogram loss is defined as the cross-entropy between the predicted distribution and the target bin (one-hot) derived from the target coordinates:

$$\mathcal{L}_{\text{disto}} = -\mathbb{E}_{\mathbf{x}_t} \left[ \frac{1}{L^2} \sum_{i,j=1}^L \sum_{b=1}^{64} \delta_{(i,j)}^{(b)}(\mathbf{x}_t) \log \mathbf{P}_{\theta,(i,j)}^{(b)}(\mathbf{z}_{t,(i,j)}) \right], \quad (10)$$

where  $\delta_{(i,j)}^{(b)}(\mathbf{x}_t)$  indicates whether the distance between tokens  $i$  and  $j$  in the target structure falls into the bin  $b$ , and the target frame  $\mathbf{x}_t$  is sampled via the training regime above.

*Reconstruction Loss (Denoising Diffusion).* This objective optimizes the diffusion-based decoder  $\mathcal{D}_\theta$  to (conditionally) recover the target frame  $\mathbf{x}_t$  from a noise-corrupted state  $\tilde{\mathbf{x}}^{(\gamma)}$ . Firstly, we parameterize the decoder  $\mathcal{D}_\theta$  using an EDM-style diffusion process (Karras et al., 2022). During training, the noisy state is sampled following the diffusion time schedule  $\gamma \sim p(\gamma) \in \mathbb{R}^+$ :

$$\tilde{\mathbf{x}}^{(\gamma)} = \mathbf{x}_t + \gamma \cdot \epsilon, \quad \epsilon \sim \mathcal{N}(0, \mathbf{I}). \quad (11)$$

To ensure the model focuses on non-trivial structural deviations rather than global rotations or translations, we apply the Kabsch algorithm to rigid align the target frame to the denoise coordinates. The loss is defined as:

$$\mathcal{L}_{\text{recon}} = \mathbb{E}_{\mathbf{x}_t, \gamma, \epsilon} \left[ \sum_{i=1}^N \omega(i, d, \gamma) \|\hat{\mathbf{x}}_i - \text{Align}(\mathbf{x}_{t,i})\|^2 \right] \quad (12)$$

where  $\hat{\mathbf{x}} = \mathcal{D}_\theta(\tilde{\mathbf{x}}^{(\gamma)}, \mathbf{a}, \mathbf{h}_t, \gamma)$  is the predicted denoised structure. The weighting term  $\omega(i, d, \gamma) = w_{\text{entity}}(i) \cdot w_{\text{diff}}(\gamma, \sigma_{\text{data}})$  balances the loss by accounting for: atom entities  $w_{\text{entity}}$  (distinguishes atoms from protein, ligand, etc.), dataset-specific noise scales  $\sigma_{\text{data}} > 0$ , and diffusion weighting  $w_{\text{diff}}(\gamma, \sigma_{\text{data}}) \triangleq (\gamma^2 + \sigma_{\text{data}}^2) / (\gamma \cdot \sigma_{\text{data}})^2$ .

The final training objective is a linear combination as:

$$\mathcal{L} = \lambda_{\text{recon}} \cdot \mathcal{L}_{\text{recon}} + \lambda_{\text{disto}} \cdot \mathcal{L}_{\text{disto}}, \quad (13)$$

with  $\lambda_{\text{recon}} > 0, \lambda_{\text{disto}} > 0$  as tunable hyperparameters.

### 3.5. Trajectory Sampling

**Bi-Level Sampling Protocol.** During inference, ATMOS samples trajectories in a specific temporal granularity  $\Delta t$ . However, autoregressive generation of high-dimension conformation over long horizons can lose consistency due to accumulated drift. Motivated by prior work (Henzler-Wildman & Kern, 2007; Xu et al., 2025b), we adopt a hierarchical, coarse-to-fine sampling strategy that decouples conformation changes from local fluctuations. In practice, we specialize two variants of ATMOS: a *keyframe generator*  $\mathcal{G}$  trained with a large temporal stride ( $\Delta t^{\text{kf}} \triangleq u \cdot \Delta t$ , where  $u > 1$  is an upsampling factor) to predict distinct anchor conformations, and an *interpolator*  $\mathcal{I}$  trained with a fine temporal stride ( $\Delta t$ ) to fill in the dynamics between anchors; in other words, the interpolator upsamples (with the factor  $u > 1$ ) the trajectory generated from  $\mathcal{G}$ . This bi-level approach offers a key advantage: it enables the parallel generation of fine-grained frames between anchor frames and significantly enhances sampling efficiency.

**Conditioned Interpolation.** While the keyframe generator operates via standard autoregressive rollout, the interpolator requires awareness of the ‘‘destination’’ to ensure a coherent trajectory between endpoints, i.e., adjacent anchor frames. Consequently, the interpolator variant  $\mathcal{I}$  is conditioned on not only the starting frame  $\mathbf{x}_t$ , but also the subsequent anchor frame  $\mathbf{x}_{t'}$  (with  $t' = t + \Delta t^{\text{kf}}$ ) and the remaining time horizon:  $p_\theta(\mathbf{x}_{t:t'} | \mathbf{x}_t, \mathbf{x}_{t'}, \mathbf{a}) = \prod_{k=1}^u p_\theta(\mathbf{x}_{t+k\Delta t} | \mathbf{x}_{t:t+(k-1)\Delta t}, \mathbf{x}_{t'}, \mathbf{a}, t_{\text{rem}})$ , where  $t_{\text{rem}} \equiv (u - k + 1)\Delta t$  is the temporal distance between the current and the next anchor frame.

## 4. Experiments

### 4.1. Experimental Settings

**Dataset.** We evaluate ATMOS on two modalities: single protein dynamics and protein-ligand dynamics. For protein dynamics, we adopt the mdCATH dataset (Mirarchi et al., 2024), which provides molecular dynamics simulations for a wide range of protein domains. mdCATH features simulations of 5,398 domains at five different temperatures, each with five replicas, offering a large-scale, statistically robust

Table 1. **Evaluation on mdCATH.** The best scores are highlighted in **bold** and the second-best scores are underlined.  $r$ : Pearson correlation;  $J$ : Jaccard similarity;  $\mathcal{W}_2$ : 2-Wasserstein distance.

		Conformation Models		Trajectory Models				Reference
		AlphaFlow-MD	ESMFlow-MD	MDGen	TEMPO	ConfRover	ATMOS	MD traj.
Predicting flexibility	Pairwise RMSD $r \uparrow$	0.61	0.46	0.65	<u>0.73</u>	0.69	<b>0.92</b>	0.96
	Global RMSF $r \uparrow$	0.57	0.47	<u>0.67</u>	0.61	0.62	<b>0.90</b>	0.95
	Per-target RMSF $r \uparrow$	<u>0.85</u>	0.80	0.77	0.52	0.81	<b>0.89</b>	0.95
Distributional accuracy	Root mean $\mathcal{W}_2$ -dist. $\downarrow$	<u>3.40</u>	5.00	3.86	4.98	4.52	<b>2.70</b>	1.89
	MD PCA $\mathcal{W}_2$ -dist. $\downarrow$	2.26	<u>2.16</u>	2.75	2.38	3.04	<b>1.79</b>	1.67
	Joint PCA $\mathcal{W}_2$ -dist. $\downarrow$	<u>3.07</u>	4.20	3.54	4.71	4.15	<b>2.32</b>	1.75
	% PC-sim $> 0.5 \uparrow$	<u>35.5</u>	25.8	3.17	7.94	22.2	<b>47.6</b>	61.9
Ensemble observables	Weak contacts $J \uparrow$	0.51	0.50	<u>0.57</u>	0.48	0.43	<b>0.65</b>	0.84
	Transient contacts $J \uparrow$	<u>0.29</u>	0.26	0.22	0.20	0.22	<b>0.38</b>	0.55
Trajectory	t-RMSD Error $\downarrow$	-	-	2.71	<u>2.42</u>	2.50	<b>1.79</b>	0.00

perspective on protein structural dynamics under varying conditions. The simulations are sampled at 1ns intervals. We follow the dataset construction of TEMPO (Xu et al., 2025b), which focuses on 320K trajectories and uses 1,000 domains for training, 50 for validation, and 64 for testing, with an average sequence similarity of 18.93% between the training and test sets, ensuring a challenging generalization benchmark. For protein–ligand dynamics, we use the MIS-ATO dataset (Siebenmorgen et al., 2024), which provides trajectories capturing the coupled dynamics of proteins and ligands. The simulations are performed at 300 K for 8 ns, yielding 100 snapshots per trajectory. We preprocess MIS-ATO following a procedure similar to Boltz-2 (Passaro et al., 2025), resulting in 12,786 systems for training, 1,278 for validation, and 1,289 for testing (see Appendix C for preprocessing details). Due to the computational cost of trajectory generation, we randomly sample 100 systems from the test set for final evaluation, aligning the test scale with Boltz-2 and yielding final splits of 12,786 (train), 1,278 (val), and 100 (test). The PDB IDs of the sampled test systems are provided in Appendix C.

**Implementation details.** We initialize ATMOS with biomolecular structural priors by leveraging pre-trained modules from Protenix (Chen et al., 2025), an open-source reproduction of AlphaFold3 (Abramson et al., 2024). Specifically, the context embedding layer that maps atom and residue attributes to the initial latent state  $\mathbf{h}_0 \triangleq (\mathbf{s}_0, \mathbf{z}_0) = \mathbf{e}_\theta(\mathbf{a})$ , as well as the diffusion decoder  $\mathcal{D}_\theta$ , are initialized with weights from Protenix. These modules provide an effective prior on plausible biomolecular geometries, enabling data-efficient learning of dynamics. The remaining components—the geometric encoder  $\mathcal{E}_\theta$  and the state-transition kernel  $\mathcal{T}_\theta$ —are trained from scratch. Architectural details of these modules are provided in the Appendix A.

We adopt the dual-scale generation strategy described in Section 3.5. On the mdCATH dataset, we train two separate models: one for coarse-scale keyframe generation at a 20ns

interval and another for fine-scale interpolation at a 1ns interval. Similarly, for MISATO, we train a coarse model at 0.8ns and a fine model at 0.08ns. This yields four trained models in total; we leave the exploration of a unified model for future work. Complete training hyperparameter settings are listed in the Appendix D.

## 4.2. Protein Dynamics

**Baselines.** We compare ATMOS with three recent trajectory generation models: MDGEN (Jing et al., 2024b), TEMPO (Xu et al., 2025b), and ConfRover (Shen et al., 2025). MDGEN and TEMPO are trained on mdCATH, while for ConfRover (which only provides inference code) we use the checkpoint trained on the ATLAS dataset (Van-der Meersche et al., 2024). Additionally, we include two SOTA conformation generation models, AlphaFlow-MD and ESMFlow-MD (Jing et al., 2024a), which generate equilibrium ensembles without temporal correlations.

**Setup.** For each protein in the test set, we condition on the initial structure and generate a trajectory of 400 frames at 1ns intervals, which we then compare to the corresponding MD reference trajectory. For the conformation generation baselines (AlphaFlow-MD and ESMFlow-MD), we generate an independent set of conformations of equal size for comparison. Our evaluation follows the protocol of AlphaFlow (Jing et al., 2024a), which assesses three aspects: flexibility prediction, distributional accuracy, and ensemble observables. Additionally, following TEMPO (Xu et al., 2025b), we report the t-RMSD Error, a trajectory-level metric that quantifies a model’s ability to reproduce the magnitude of conformational change over time. This metric is computed by (1) calculating the RMSD of each frame to the initial frame, and (2) computing the RMSE between the resulting RMSD sequences of the predicted and ground-truth trajectories. Detailed definitions and explanations of all metrics are provided in the Appendix E.

**Results.** As shown in Table 1, ATMOS achieves state-of-the-

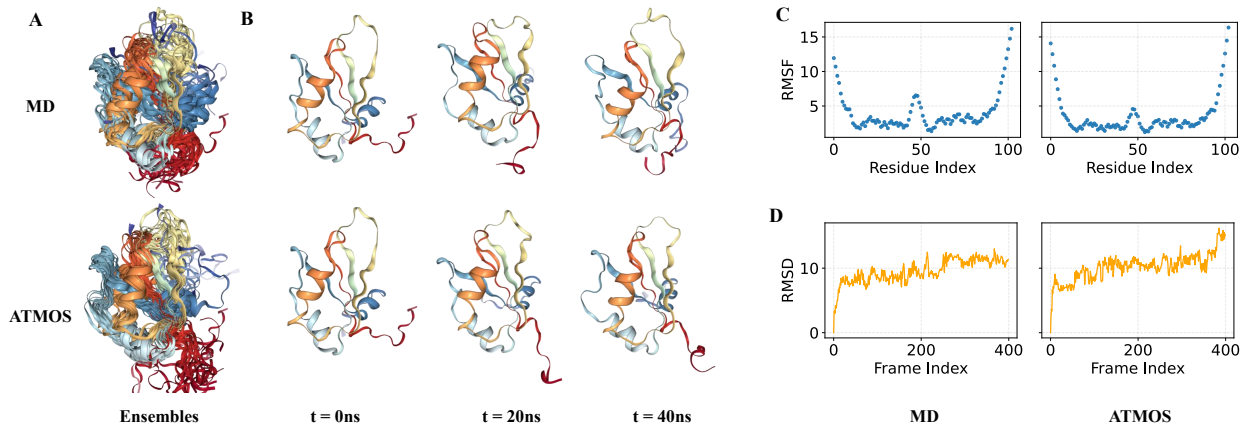


Figure 2. Case Study on *1s79a00*, a target from the test set of mdCATH. (A) the visualization of ensemble from MD simulation (reference) or ATMOS (sampled). (B) The visualization of snapshot at specific frame index. (C) The RMSF versus the residue index. (D) The moving RMSD to the initial structure (frame 0) along the trajectory frames.

art performance across all evaluation metrics, demonstrating its ability to generate high-quality, physically realistic protein dynamics. On the flexibility prediction tasks, ATMOS significantly outperforms both conformation models and previous trajectory models, achieving a near-perfect correlation with the reference MD trajectories in pairwise RMSD (Pearson  $r = 0.92$ ) and global RMSF ( $r = 0.90$ ). This indicates that our model accurately captures both the overall conformational diversity and the local atomic fluctuations present in real dynamics. In terms of distributional accuracy, ATMOS consistently produces ensembles that are closer to the reference distribution than any baseline, as evidenced by the lowest Wasserstein distances across all three PCA-based metrics and the highest percentage of similar principal components (47.6%). Notably, it reduces the root mean 2-Wasserstein distance to  $2.7\text{\AA}$ , a substantial improvement over the second-best conformation model (AlphaFlow-MD,  $3.40\text{\AA}$ ) and the best prior trajectory model (MDGEN,  $3.86\text{\AA}$ ). This shows that ATMOS sample the correct principal motion patterns. For ensemble observables, ATMOS also excels, achieving the highest Jaccard similarity for both weak contacts and transient contacts, which are critical for understanding functional dynamics. Finally, on the trajectory-specific metric t-RMSD Error, ATMOS attains a value of  $1.79\text{\AA}$ , significantly lower than the best prior trajectory model. This result underscores the advantage of our state-space modeling approach in maintaining coherent, long-range temporal evolution.

Overall, the results validate that ATMOS successfully bridges the gap between static structural priors and dynamic trajectory generation, offering a unified framework that captures both the equilibrium distribution and the kinetic pathways of protein dynamics. We further visualize one representative case in Figure 2.

Table 2. Efficiency evaluation on the *1glna01* protein (139 AA). MD simulation is performed with Amber24 on GPU (Salomon-Ferrer et al., 2013), employing an integration time step of 4 fs.

Model	Inference Time (Hour)	Peak Mem (GB)
MD Simulation	>10	<1
ConfRover	0.467	22.53
ATMOS	0.174	3.445
ATMOS-Parallel	0.044	6.117

**Efficiency.** We evaluate the inference efficiency of ATMOS on the *1glna01* protein (139AA) by generating a 400ns trajectory (400 frames at 1ns intervals). As shown in Table 2, ATMOS achieves superior efficiency by leveraging state-space models, which capture long-range temporal dependencies with linear complexity in trajectory length. We compare against two representative baselines: traditional MD simulation and ConfRover, which employs a causal transformer that must revisit the history for each prediction, leading to quadratic scaling. All methods are run on a single RTX 4090 GPU. ATMOS reduces inference time by  $2.7\times$  compared to ConfRover and by over  $60\times$  compared to MD simulation, while using only 15% of ConfRover’s peak memory. By parallelizing the interpolation step across the batch dimension (ATMOS-Parallel), inference time is further reduced by  $4\times$  at a modest increase in memory. These results validate that our SSM-based framework offers a compelling reduction in computational cost, enabling scalable generation of long, all-atom trajectories.

### 4.3. Protein-Ligand Dynamics

**Baselines.** For protein-ligand dynamics, we compare with GNNMD (Siebenmorgen et al., 2024), DenoisingLD (Wu & Li, 2023), NeuralMD and VerletMD (Liu et al., 2025), DynamicBind (Lu et al., 2024b), and Boltz-2 (Passaro et al.,

Table 3. **Evaluation on MISATO.** The best scores are highlighted in **bold** and the second-best scores are underlined.  $r$ : Pearson correlation;  $\mathcal{W}_2$ : 2-Wasserstein distance. Boltz-2 is trained on the entire MISATO dataset, which may lead to data leakage; we include it as a strong but potentially optimistic baseline.

Method	per-target RMSF $r \uparrow$	Root mean $\mathcal{W}_2$ -dist $\downarrow$	Steric Clashes $\downarrow$	t-RMSD Error $\downarrow$	
Ligand	DenosingLD (Wu & Li, 2023)	0.028	0.791	1.825	34.01
	GNNMD (Siebenmorgen et al., 2024)	0.135	0.870	81.69	<u>0.672</u>
	NeuralMD-SDE (Liu et al., 2025)	0.574	<u>0.698</u>	7.667	0.698
	VerletMD (Liu et al., 2025)	0.456	36.83	14.67	43.78
	DynamicBind (Lu et al., 2024b)	<u>0.678</u>	1.470	7.113	-
	Boltz-2 (Passaro et al., 2025)	0.613	1.237	<u>0.210</u>	-
	ATMOS (ours)	<b>0.746</b>	<b>0.670</b>	<b>0.030</b>	<b>0.480</b>
Protein-Ligand	DynamicBind (Lu et al., 2024b)	0.193	2.288	52.74	-
	Boltz-2 (Passaro et al., 2025)	<b>0.534</b>	<u>1.992</u>	<b>0.020</b>	-
	ATMOS (ours)	<u>0.523</u>	<b>1.567</b>	<u>0.051</u>	<b>0.600</b>

2025). The first four models focus on ligand dynamics within the complex, while the latter two generate conformational ensembles for the entire protein–ligand system.

**Setup.** Similar to the evaluation protocol for mdCATH, we condition on the initial structure and generate the full trajectory. For the conformation generation baselines (DynamicBind and Boltz-2), we generate an independent set of conformations of equal size for comparison. We assess four aspects: flexibility prediction (per-target RMSF Pearson correlation), distributional accuracy (root mean 2-Wasserstein distance), steric clashes, and trajectory accuracy (t-RMSD Error). Detailed metric definitions are provided in Appendix E. Two important notes: (1) Since the first four baselines model only ligand dynamics, we report separate results for ligand-only and (where applicable) whole-system evaluations. (2) Boltz-2 is trained on the entire MISATO dataset, which may lead to data leakage; we include it as a strong but potentially optimistic baseline.

**Results.** As shown in Table 3, ATMOS achieves strong performance across both ligand-only and full protein–ligand evaluations. For ligand dynamics, ATMOS attains the best scores in all four metrics. These results demonstrate that our model generates physically realistic ligand motions while closely matching the reference distribution and temporal evolution. On the full protein–ligand system, ATMOS delivers competitive performance: it obtains the second-best RMSF correlation and clash count, while achieving the best Wasserstein distance. Notably, ATMOS is the only method that reports an t-RMSD Error for the entire complex, highlighting its ability to model coupled protein–ligand dynamics with temporal coherence. Although Boltz-2 shows slightly better performance on some metrics, it is trained on the entire dataset (potential data leakage) and does not produce trajectories, thus lacking any measure of temporal accuracy. In summary, ATMOS not only excels at modeling ligand-in-pocket dynamics but also provides a unified framework for generating coherent, all-atom trajectories of the entire protein–ligand system.

Table 4. **Ablation study on sampling protocol.**

Metric	ATMOS	w/o bi-level sampling	ODE
Pairwise RMSD $r \uparrow$	<b>0.92</b>	0.88	0.73
Global RMSF $r \uparrow$	<b>0.90</b>	0.84	0.64
Per-target RMSF $r \uparrow$	<b>0.89</b>	0.85	0.63
Root mean $\mathcal{W}_2$ -dist. $\downarrow$	<b>2.70</b>	3.06	3.89
MD PCA $\mathcal{W}_2$ -dist. $\downarrow$	<b>1.79</b>	2.09	2.73
Joint PCA $\mathcal{W}_2$ -dist. $\downarrow$	<b>2.32</b>	2.61	3.28
% PC-sim > 0.5 $\uparrow$	<b>47.6</b>	39.1	17.2
Weak contacts $J \uparrow$	<b>0.65</b>	0.56	0.26
Transient contacts $J \uparrow$	<b>0.38</b>	0.31	0.20
t-RMSD Error $\downarrow$	<b>1.79</b>	2.03	3.22

#### 4.4. Ablation Study

We ablate two key sampling configurations in ATMOS: the bi-level sampling protocol and the stochasticity of the EDM-based diffusion sampling (Karras et al., 2022). Results on mdCATH (Table 4) show that removing the hierarchical generation strategy degrades performance across all metrics, confirming that generating coarse keyframes before interpolation reduces error accumulation and improves long-range consistency. Replacing the SDE (see Algorithm 4) with a deterministic ODE flow (see Appendix A.3) similarly causes a pronounced drop in ensemble quality. This demonstrates that stochastic diffusion is essential for capturing the thermal diversity of biomolecular conformations.

## 5. Conclusion

We present ATMOS, a unified generative framework for simulating biomolecular dynamics that generalizes from monomeric proteins to complex biomolecular systems. ATMOS operates at the all-atom level and adapts state-space models to trajectory generation, enabling efficient capture of long-range temporal dependencies with linear inference complexity. The model achieves SOTA performance on large-scale MD benchmarks, demonstrating its ability to generalize across diverse biological systems and paving the way toward foundational dynamics models.

## Impact Statement

ATMOS has significant broader impacts for computational biology and drug discovery. It provides a general-purpose framework for modeling biomolecular dynamics that could accelerate therapeutic discovery and enhance biological understanding. However, ethical concerns, such as potential misuse in drug development, warrant careful consideration. Responsible deployment and transparency are essential to maximize benefits and mitigate risks.

## References

- Abramson, J., Adler, J., Dunger, J., Evans, R., Green, T., Pritzel, A., Ronneberger, O., Willmore, L., Ballard, A. J., Bambrick, J., et al. Accurate structure prediction of biomolecular interactions with alphafold 3. *Nature*, 630 (8016):493–500, 2024.
- Chen, X., Zhang, Y., Lu, C., Ma, W., Guan, J., Gong, C., Yang, J., Zhang, H., Zhang, K., Wu, S., et al. Protenix-advancing structure prediction through a comprehensive alphafold3 reproduction. *bioRxiv*, pp. 2025–01, 2025.
- Costa, A. D. S., Mitnikov, I., Pellegrini, F., Daigavane, A., Geiger, M., Cao, Z., Kreis, K., Smidt, T., Kucukbenli, E., and Jacobson, J. Equijump: Protein dynamics simulation via so (3)-equivariant stochastic interpolants. *arXiv preprint arXiv:2410.09667*, 2024.
- Del Alamo, D., Sala, D., Mchaourab, H. S., and Meiler, J. Sampling alternative conformational states of transporters and receptors with alphafold2. *Elife*, 11:e75751, 2022.
- Feng, B., Zhang, J., Zhang, X., Liu, Z., and Li, Y. Biomd: All-atom generative model for biomolecular dynamics simulation. *arXiv preprint arXiv:2509.02642*, 2025.
- Gu, A., Goel, K., and Ré, C. Efficiently modeling long sequences with structured state spaces. *arXiv preprint arXiv:2111.00396*, 2021a.
- Gu, A., Johnson, I., Goel, K., Saab, K., Dao, T., Rudra, A., and Ré, C. Combining recurrent, convolutional, and continuous-time models with linear state space layers. *Advances in neural information processing systems*, 34: 572–585, 2021b.
- Henzler-Wildman, K. and Kern, D. Dynamic personalities of proteins. *Nature*, 450(7172):964–972, 2007.
- Jing, B., Berger, B., and Jaakkola, T. AlphaFold meets flow matching for generating protein ensembles. In Salakhutdinov, R., Kolter, Z., Heller, K., Weller, A., Oliver, N., Scarlett, J., and Berkenkamp, F. (eds.), *Proceedings of the 41st International Conference on Machine Learning*, volume 235 of *Proceedings of Machine Learning Research*, pp. 22277–22303. PMLR, 21–27 Jul 2024a. URL <https://proceedings.mlr.press/v235/jing24a.html>.
- Jing, B., Stärk, H., Jaakkola, T., and Berger, B. Generative modeling of molecular dynamics trajectories. *Advances in Neural Information Processing Systems*, 37:40534–40564, 2024b.
- Jumper, J., Evans, R., Pritzel, A., Green, T., Figurnov, M., Ronneberger, O., Tunyasuvunakool, K., Bates, R., Žídek, A., Potapenko, A., et al. Highly accurate protein structure prediction with alphafold. *nature*, 596(7873):583–589, 2021.
- Karras, T., Aittala, M., Aila, T., and Laine, S. Elucidating the design space of diffusion-based generative models. *Advances in neural information processing systems*, 35: 26565–26577, 2022.
- Klein, L., Foong, A., Fjelde, T., Mlodozieniec, B., Brockschmidt, M., Nowozin, S., Noé, F., and Tomioka, R. Timewarp: Transferable acceleration of molecular dynamics by learning time-coarsened dynamics. *Advances in Neural Information Processing Systems*, 36:52863–52883, 2023.
- Lewis, S., Hempel, T., Jiménez-Luna, J., Gastegger, M., Xie, Y., Foong, A. Y., Satorras, V. G., Abdin, O., Veeling, B. S., Zaporozhets, I., et al. Scalable emulation of protein equilibrium ensembles with generative deep learning. *Science*, 389(6761):eadv9817, 2025.
- Liu, S., Du, W., Xu, H., Li, Y., Li, Z., Bhethanabotla, V., Yan, D., Borgs, C., Anandkumar, A., Guo, H., et al. A multi-grained symmetric differential equation model for learning protein-ligand binding dynamics. *Nature Communications*, 2025.
- Lu, J., Zhong, B., Zhang, Z., and Tang, J. Str2str: A score-based framework for zero-shot protein conformation sampling. In *The Twelfth International Conference on Learning Representations*, 2024a. URL <https://openreview.net/forum?id=C4BikKsgmK>.
- Lu, J., Chen, X., Lu, S. Z., Lozano, A., Chenthamarashan, V., Das, P., and Tang, J. Aligning protein conformation ensemble generation with physical feedback. In Singh, A., Fazel, M., Hsu, D., Lacoste-Julien, S., Berkenkamp, F., Maharaj, T., Wagstaff, K., and Zhu, J. (eds.), *Proceedings of the 42nd International Conference on Machine Learning*, volume 267 of *Proceedings of Machine Learning Research*, pp. 40436–40451. PMLR, 13–19 Jul 2025a. URL <https://proceedings.mlr.press/v267/lu25b.html>.

- Lu, J., Chen, X., Lu, S. Z., Shi, C., Guo, H., Bengio, Y., and Tang, J. Structure language models for protein conformation generation. In *The Thirteenth International Conference on Learning Representations*, 2025b. URL <https://openreview.net/forum?id=OzUNdnpQyd>.
- Lu, W., Zhang, J., Huang, W., Zhang, Z., Jia, X., Wang, Z., Shi, L., Li, C., Wolynes, P. G., and Zheng, S. Dynamibind: predicting ligand-specific protein-ligand complex structure with a deep equivariant generative model. *Nature Communications*, 15(1):1071, 2024b.
- McGibbon, R. T., Beauchamp, K. A., Harrigan, M. P., Klein, C., Swails, J. M., Hernández, C. X., Schwantes, C. R., Wang, L.-P., Lane, T. J., and Pande, V. S. Mdtraj: a modern open library for the analysis of molecular dynamics trajectories. *Biophysical journal*, 109(8):1528–1532, 2015.
- Mirarchi, A., Giorgino, T., and De Fabritiis, G. mdcat: A large-scale md dataset for data-driven computational biophysics. *Scientific Data*, 11(1):1299, 2024.
- Noé, F., Olsson, S., Köhler, J., and Wu, H. Boltzmann generators: Sampling equilibrium states of many-body systems with deep learning. *Science*, 365(6457):eaaw1147, 2019.
- Passaro, S., Corso, G., Wohlwend, J., Reveiz, M., Thaler, S., Somnath, V. R., Getz, N., Portnoi, T., Roy, J., Stark, H., et al. Boltz-2: Towards accurate and efficient binding affinity prediction. *BioRxiv*, 2025.
- Salomon-Ferrer, R., Gotz, A. W., Poole, D., Le Grand, S., and Walker, R. C. Routine microsecond molecular dynamics simulations with amber on gpus. 2. explicit solvent particle mesh ewald. *Journal of chemical theory and computation*, 9(9):3878–3888, 2013.
- Schreiner, M., Winther, O., and Olsson, S. Implicit transfer operator learning: Multiple time-resolution models for molecular dynamics. *Advances in Neural Information Processing Systems*, 36:36449–36462, 2023.
- Shen, Y., Wang, L., Yuan, H., Wang, Y., Yang, B., and Gu, Q. Simultaneous modeling of protein conformation and dynamics via autoregression. In *ICML 2025 Generative AI and Biology (GenBio) Workshop*, 2025. URL <https://openreview.net/forum?id=BaZL1cQzV0>.
- Siebenmorgen, T., Menezes, F., Benassou, S., Merdivan, E., Didi, K., Mourão, A. S. D., Kitel, R., Liò, P., Kesselheim, S., Piraud, M., et al. Misato: machine learning dataset of protein–ligand complexes for structure-based drug discovery. *Nature computational science*, 4(5):367–378, 2024.
- Vander Meersche, Y., Cretin, G., Gheeraert, A., Gelly, J.-C., and Galochkina, T. Atlas: protein flexibility description from atomistic molecular dynamics simulations. *Nucleic acids research*, 52(D1):D384–D392, 2024.
- Wang, Y., Wang, L., Shen, Y., Wang, Y., Yuan, H., Wu, Y., and Gu, Q. Protein conformation generation via force-guided se (3) diffusion models. *arXiv preprint arXiv:2403.14088*, 2024.
- Wayment-Steele, H. K., Ojoawo, A., Otten, R., Apitz, J. M., Pitsawong, W., Hömberger, M., Ovchinnikov, S., Colwell, L., and Kern, D. Predicting multiple conformations via sequence clustering and alphafold2. *Nature*, 625(7996):832–839, 2024.
- Williams, R. J. and Zipser, D. A learning algorithm for continually running fully recurrent neural networks. *Neural computation*, 1(2):270–280, 1989.
- Wu, F. and Li, S. Z. Diffmd: a geometric diffusion model for molecular dynamics simulations. In *Proceedings of the AAAI conference on artificial intelligence*, volume 37, pp. 5321–5329, 2023.
- Xu, K., Wang, J., Liu, M., Zhou, K., Lin, S., Li, W., Shi, L., Zhou, P., Liu, H., and Yao, X. Efficient generation of protein and protein–protein complex dynamics via se(3)-parameterized diffusion models. *Journal of Chemical Information and Modeling*, 65(22):12366–12376, 2025a.
- Xu, Y., Wang, D., Zhou, Z., Yu, T., and Chen, M. TEMPO: Temporal multi-scale autoregressive generation of protein conformational ensembles. In *The Thirty-ninth Annual Conference on Neural Information Processing Systems*, 2025b. URL <https://openreview.net/forum?id=0wV5HR7M4P>.
- Zheng, S., He, J., Liu, C., Shi, Y., Lu, Z., Feng, W., Ju, F., Wang, J., Zhu, J., Min, Y., et al. Predicting equilibrium distributions for molecular systems with deep learning. *Nature Machine Intelligence*, 6(5):558–567, 2024.

## A. Architectural Details

This section provides implementation details for the key modules introduced in Section 3.3.

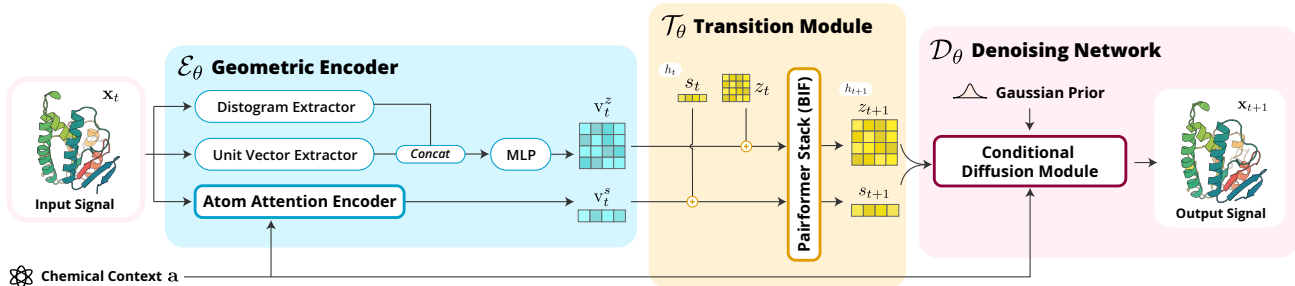


Figure 3. Detailed architecture of our framework. BIF: Bidirectional Information Flow.

### A.1. Context and Input Encoding

We initialize the context embedding layer  $e_\theta$  with the pre-trained trunk module of Protenix (Chen et al., 2025) (an open-source reproduction of AlphaFold3 (Abramson et al., 2024)), which includes the Input Feature Embedder, MSA Module and Pairformer. This module is fine-tuned during training.

The geometric encoder  $\mathcal{E}_\theta$  maps the current all-atom conformation  $X_t$  into a forcing term  $\mathbf{v}_t = (\mathbf{v}_t^s, \mathbf{v}_t^z)$  that captures both global topology and local atomic details. Consistent with the dual-track latent representation,  $\mathcal{E}_\theta$  decomposes structural information into a token-level single representation  $\mathbf{v}_t^s \in \mathbb{R}^{L \times d_s}$  and a pairwise representation  $\mathbf{v}_t^z \in \mathbb{R}^{L \times L \times d_z}$ , where  $L$  denotes the length of the tokenized sequence.

**Pairwise geometric features.** For each token pair  $(i, j)$ , we compute invariant features that encode their relative geometry. For protein residues, the token center is taken as the  $C\beta$  atom ( $C\alpha$  for glycine); for ligand atoms, the atom itself serves as the center. We compute (1) a distance histogram between the two centers, and (2) unit vectors that express the displacement vector in the local coordinate frame of each token (constructed from backbone atoms for residues and neighboring atoms for ligands). These features are concatenated and projected:

$$\mathbf{v}_t^z[i, j] = \text{MLP}(\text{concat}(\text{Distogram}_{ij}, \text{UnitVectors}_{ij})). \quad (14)$$

**Token-wise local encoding.** To capture detailed side-chain conformations and local chemical environments, we employ an AtomAttentionEncoder (Algorithm 1) similar to the one in AlphaFold3 (Abramson et al., 2024)). This module processes the current all-atom structure  $X_t$  and summarizes intra-token atomic arrangements and their neighborhoods into a fixed-dimensional token-wise representation:

$$\mathbf{v}_t^s = \text{AtomAttentionEncoder}(X_t, \mathbf{a}). \quad (15)$$

Pseudocode for the AtomAttentionEncoder submodules (e.g., AtomTransformer) follows the description in the AlphaFold 3 supplementary material (Abramson et al., 2024).

Together,  $\mathbf{v}_t^s$  and  $\mathbf{v}_t^z$  provide a comprehensive geometric encoding that serves as the forcing term to the state transition module.

### A.2. State Transition

The core propagator of ATMOS is the state transition function  $\mathcal{T}_\theta$ , which evolves the latent state  $\mathbf{h}$  from  $t$  to  $t + 1$ . We instantiate  $\mathcal{T}_\theta$  as a variant of the Pairformer module (Algorithm 2) (Abramson et al., 2024), which is uniquely suited for this role because it enables bidirectional information flow between the single and pair tracks. For reference, we provide the original Pairformer pseudocode in Algorithm 3 and highlight the modifications in Algorithm 2. Pseudocode for the Pairformer submodules (e.g., TriangleMultiplicationOutgoing, TriangleAttentionStartingNode) follows the description in the AlphaFold 3 supplementary material (Abramson et al., 2024). We use 4 Pairformer blocks in our implementation. The architectural hyperparameters are listed in Table 5.

**Algorithm 1** Atom Attention Encoder

---

```

1: Input: all-atom coordinate  $\mathbf{x} \in \mathcal{R}^{N \times 3}$ , Chemical Context  $\mathbf{a}$ .
2: Output: forcing term  $\mathbf{v}^s \in \mathcal{R}^{N \times d^s}$ .
3:  $\mathbf{c}_i \leftarrow \text{LinearNoBias}(\text{concat}(\mathbf{x}_i, \mathbf{a}_i^{\text{atom\_charge}}, \mathbf{a}_i^{\text{atom\_element}}, \mathbf{a}_i^{\text{atom\_name}}))$ 
4:  $\mathbf{d}_{ij} \leftarrow \mathbf{x}_i - \mathbf{x}_j$ 
5:  $\mathbf{m}_{ij} \leftarrow 1.0$  if atom  $i, j$  are located in the same token else 0.0
6:  $\mathbf{p}_{ij} \leftarrow \text{LinearNoBias}(\mathbf{d}_{ij}) \cdot \mathbf{m}_{ij}$ 
7:  $\mathbf{p}_{ij} \leftarrow \mathbf{p}_{ij} + \text{LinearNoBias}(1/(1 + \|\mathbf{d}_{ij}\|_2^2)) \cdot \mathbf{m}_{ij}$ 
8:  $\mathbf{p}_{ij} \leftarrow \mathbf{p}_{ij} + \text{LinearNoBias}(\mathbf{m}_{ij}) \cdot \mathbf{m}_{ij}$ 
9:  $\mathbf{p}_{ij} \leftarrow \mathbf{p}_{ij} + \text{LinearNoBias}(\text{ReLU}(\mathbf{c}_i)) + \text{LinearNoBias}(\text{ReLU}(\mathbf{c}_j))$ 
10:  $\mathbf{p}_{ij} \leftarrow \mathbf{p}_{ij} + \text{MLP}(\mathbf{p}_{ij})$ 
11:  $\mathbf{q} \leftarrow \text{AtomTransformer}(\mathbf{q}, \mathbf{p})$  # Atom local attention; same architecture as AlphaFold 3;  $\mathbf{p}$  is the pair bias.
12:  $\mathbf{v}^s \leftarrow \text{mean\_pooling}(\mathbf{q})$  # Pool atom-level representation into token-level representation.
13: Return  $\mathbf{v}^s$ 

```

---

Table 5. Architectural hyperparameters for the modified Pairformer.

Hyperparameter	Value
Number of Pairformer blocks	4
Single representation dimension	384
Pair representation dimension	128
Triangle multiplication hidden dimension	128
Number of triangle attention heads	4
Transition layer expanding factor	4
Pair attention dropout rate	0.25

**A.3. Structure Decoding**

We model the generation of the next frame  $\mathbf{x}_{t+1}$  as a reverse diffusion process, with a denoising network  $\mathcal{D}_\theta$  that predicts the clean structure from a noisy state. The diffusion decoder  $\mathcal{D}_\theta$  is initialized from the weights of Protenix (Chen et al., 2025). Together with the context embedding layer  $e_\theta$ , this provides a strong prior on plausible biomolecular geometries, enabling data-efficient learning of dynamics. We parameterize the decoder  $\mathcal{D}_\theta$  using an EDM-style diffusion process (Karras et al., 2022). The conditional diffusion sampling procedure is detailed in Algorithm 4. We use  $N_{\text{step}} = 50$  diffusion steps, a step scaling factor  $\eta = 1.5$ , and a noise scaling schedule parameter  $\gamma_0 = 0.8$  with a minimum  $\gamma_{\text{min}} = 1.0$ . The noise scaling factor  $\lambda$  is set to 1.5 for mdCATH (to encourage diversity) and 1.003 for MISATO.

Note that the stochastic differential equation (SDE) in Algorithm 4 can be converted to a deterministic ordinary differential equation (ODE) by setting  $\gamma_0 = 0$ , as done in the ablation study.

**B. Inference**

We detail the bi-level sampling protocol introduced in Section 3.5. The procedure, summarized in Algorithm 5, consists of two stages: (1) generating a sparse set of keyframes at a coarse time resolution, and (2) filling in the intermediate frames via parallel interpolation conditioned on the adjacent keyframes.

In the keyframe generation stage (lines7-13), the model autoregressively predicts a sequence of anchor conformations spaced by  $\Delta t^{\text{kf}} = u\Delta t$ . Each step encodes the last generated frame, updates the latent state, and samples a new keyframe via diffusion. In the interpolation stage (lines15-30), for each pair of consecutive keyframes ( $\mathbf{x}_{\text{start}}, \mathbf{x}_{\text{end}}$ ), we generate  $u - 1$  intermediate frames at the fine resolution  $\Delta t$ . Crucially, the interpolator’s transition function  $\mathcal{T}_\theta$  is additionally conditioned on the encoded end frame ( $\mathbf{v}_{\text{end}}^s, \mathbf{v}_{\text{end}}^z$ ) and the remaining time `rem.times`, ensuring that the generated path remains coherent with the destination. This design allows all intermediate frames within an interval to be generated in parallel, significantly accelerating sampling while maintaining trajectory consistency.

**Algorithm 2** PairformerStack with Bidirectional Information Flow

---

```

1: Input: single representation  $\mathbf{s}$ , pair representation  $\mathbf{z}$ , pairformer block number  $N_{\text{block}}$ 
2: Output: updated single representation  $\mathbf{s}$ , pair representation  $\mathbf{z}$ .
3: for  $l \in [1, \dots, N_{\text{block}}]$  do
4:    $\{\mathbf{z}_{ij}\} \leftarrow \{\mathbf{z}_{ij}\} + \{\mathbf{s}_i\} + \{\mathbf{s}_j\}$ 
5:    $\{\mathbf{z}_{ij}\} \leftarrow \{\mathbf{z}_{ij}\} + \text{DropoutRowwise}_{0.25}(\text{TriangleMultiplicationOutgoing}(\{\mathbf{z}_{ij}\}))$ 
6:    $\{\mathbf{z}_{ij}\} \leftarrow \{\mathbf{z}_{ij}\} + \text{DropoutRowwise}_{0.25}(\text{TriangleMultiplicationIncoming}(\{\mathbf{z}_{ij}\}))$ 
7:    $\{\mathbf{z}_{ij}\} \leftarrow \{\mathbf{z}_{ij}\} + \text{DropoutRowwise}_{0.25}(\text{TriangleAttentionStartingNode}(\{\mathbf{z}_{ij}\}))$ 
8:    $\{\mathbf{z}_{ij}\} \leftarrow \{\mathbf{z}_{ij}\} + \text{DropoutColumnwise}_{0.25}(\text{TriangleAttentionEndingNode}(\{\mathbf{z}_{ij}\}))$ 
9:    $\{\mathbf{z}_{ij}\} \leftarrow \{\mathbf{z}_{ij}\} + \text{Transition}(\{\mathbf{z}_{ij}\})$ 
10:   $\{\mathbf{s}_i\} \leftarrow \{\mathbf{s}_i\} + \text{AttentionPairBias}(\{\mathbf{s}_i\}, \{\mathbf{z}_{ij}\})$ 
11:   $\{\mathbf{s}_i\} \leftarrow \{\mathbf{s}_i\} + \text{Transition}(\{\mathbf{s}_i\})$ 
12: end for
13: Return  $\mathbf{s}, \mathbf{z}$ 

```

---

**Algorithm 3** Original AlphaFold PairformerStack

---

```

1: Input: single representation  $\mathbf{s}$ , pair representation  $\mathbf{z}$ , pairformer block number  $N_{\text{block}}$ 
2: Output: updated single representation  $\mathbf{s}$ , pair representation  $\mathbf{z}$ .
3: for  $l \in [1, \dots, N_{\text{block}}]$  do
4:    $\{\mathbf{z}_{ij}\} \leftarrow \{\mathbf{z}_{ij}\} + \text{DropoutRowwise}_{0.25}(\text{TriangleMultiplicationOutgoing}(\{\mathbf{z}_{ij}\}))$ 
5:    $\{\mathbf{z}_{ij}\} \leftarrow \{\mathbf{z}_{ij}\} + \text{DropoutRowwise}_{0.25}(\text{TriangleMultiplicationIncoming}(\{\mathbf{z}_{ij}\}))$ 
6:    $\{\mathbf{z}_{ij}\} \leftarrow \{\mathbf{z}_{ij}\} + \text{DropoutRowwise}_{0.25}(\text{TriangleAttentionStartingNode}(\{\mathbf{z}_{ij}\}))$ 
7:    $\{\mathbf{z}_{ij}\} \leftarrow \{\mathbf{z}_{ij}\} + \text{DropoutColumnwise}_{0.25}(\text{TriangleAttentionEndingNode}(\{\mathbf{z}_{ij}\}))$ 
8:    $\{\mathbf{z}_{ij}\} \leftarrow \{\mathbf{z}_{ij}\} + \text{Transition}(\{\mathbf{z}_{ij}\})$ 
9:    $\{\mathbf{s}_i\} \leftarrow \{\mathbf{s}_i\} + \text{AttentionPairBias}(\{\mathbf{s}_i\}, \{\mathbf{z}_{ij}\})$ 
10:   $\{\mathbf{s}_i\} \leftarrow \{\mathbf{s}_i\} + \text{Transition}(\{\mathbf{s}_i\})$ 
11: end for
12: Return  $\mathbf{s}, \mathbf{z}$ 

```

---

## C. MISATO Dataset Preprocessing

We preprocess the MISATO dataset following a procedure similar to Boltz-2 (Passaro et al., 2025), resulting in 12,786 systems for training, 1,278 for validation, and 1,289 for testing.

The preprocessing consists of several steps. First, we download the MD restart file (to extract bond topology) and the MD result file (which contains trajectory coordinates and can be used to infer chain\_ids). Next, we generate a (.prmtop, .nc) pair for each protein–ligand complex. The .prmtop file holds topology information and the .nc file stores the trajectory coordinates. These files are loaded with MDTraj (McGibbon et al., 2015), and each frame is exported as an individual PDB file. This method preserves complete topology (including bonds) and ensures a robust ligand representation, whereas directly constructing a PDB from the MD result file can lose atoms and introduce parsing inconsistencies.

We then add CCD (Chemical Component Dictionary) information to the loaded (.prmtop, .nc) pair, and convert them to (.pdb, .xtc) format. Systems that do not contain a MOL (ligand) residue are excluded. We also remove systems where the ligand’s atomic elements differ from those in the corresponding PDBBind MOL2 files, ensuring chemical consistency. Additionally, trajectories in which the ligand drifts more than 12Å from the protein at any frame are filtered out.

Furthermore, we remove approximately 500 systems that cannot be processed by the Protenix (Chen et al., 2025) data pipeline due to unexpected errors, indicating potential format, content, or geometry issues. (We first convert the PDB file to mmCIF format and then applies Protenix’s standard processing.) We plan to release the preprocessed MISATO dataset to support future research.

The PDB IDs of the randomly sampled test systems are as follows: 16PK, 1A08, 1D2S, 1DHJ, 1DRK, 1F73, 1IK4, 1JQD, 1NP0, 1WE2, 1XK9, 1Y2F, 1YYS, 2BET, 2EXG, 2GKL, 2HXM, 2I6B, 2LTO, 2NQI, 2PZE, 2QIC, 2RA6, 2RR4, 2V54, 2WJG, 2Y4K, 2Y4M, 2ZA3, 3BLU, 3C39, 3D9M,

**Algorithm 4** Conditional Diffusion Sampling

---

```

1: Input: Diffusion steps  $N_{\text{step}}$ , latent state  $\mathbf{h}$ , chemical context  $\mathbf{a}$ , sampling hyperparameters  $\lambda, \eta, \gamma_0, \gamma_{\text{min}}$ .
2: Output: Generated coordinates  $\mathbf{x}$ .
3: noise_schedule  $\leftarrow$  inference_noise_scheduler( $N_{\text{step}}$ )
4:  $\mathbf{x} \leftarrow$  noise_schedule[0] *  $\mathcal{N}(0, I)$  # Initialize with noise
5: for  $i \leftarrow 1$  to len(noise_schedule) do
6:    $\gamma^{\text{last}}, \gamma \leftarrow$  noise_schedule[ $i - 1$ ], noise_schedule[ $i$ ]
7:    $\mathbf{x} \leftarrow$  centre_random_augmentation( $\mathbf{x}$ ) # Apply random rigid augmentation
8:    $\gamma' \leftarrow \gamma_0$  if  $\gamma > \gamma_{\text{min}}$  else 0
9:    $t_{\text{hat}} \leftarrow \gamma^{\text{last}} * (\gamma' + 1)$ 
10:   $\mathbf{x}_{\text{noisy}} \leftarrow \mathbf{x} + \lambda \sqrt{t_{\text{hat}}^2 - (\gamma^{\text{last}})^2} * \mathcal{N}(0, I)$ 
11:   $\mathbf{x}_{\text{denoised}} \leftarrow \mathcal{D}_{\theta}(\mathbf{x}_{\text{noisy}}, \mathbf{a}, \mathbf{h}, t_{\text{hat}})$  # Conditional denoising
12:   $\delta \leftarrow (\mathbf{x}_{\text{noisy}} - \mathbf{x}_{\text{denoised}}) / t_{\text{hat}}$ 
13:   $\Delta t \leftarrow \gamma - t_{\text{hat}}$ 
14:   $\mathbf{x} \leftarrow \mathbf{x}_{\text{noisy}} + \eta * \Delta t * \delta$ 
15: end for
16: Return  $\mathbf{x}$ 

```

---

3EOR, 3F69, 3G3N, 3GPO, 3HII, 3JUQ, 3MAG, 3ME9, 3MEU, 3QVU, 3S0B, 3TNE, 3ZOT,  
4A22, 4ASK, 4AYR, 4B0C, 4DPU, 4DZY, 4G0Q, 4H7Q, 4I7B, 4KM2, 4KQO, 4KQR, 4KXL,  
4L0L, 4MRE, 4NA4, 4NRQ, 4O1L, 4O24, 4ODL, 4UFH, 4X11, 4XAQ, 4YXD, 4ZB6, 5C13,  
5C4K, 5ECT, 5EFC, 5F1R, 5H5Q, 5J6D, 5MXX, 5NPB, 5NPC, 5NPD, 5TPG, 5TT8, 5ZDC,  
6BOE, 6C3U, 6CQ5, 6CW4, 6DYN, 6DYS, 6FAC, 6FAM, 6FNR, 6FNT, 6MIN, 6NP3, 6OA3,  
6OIO, 6P12, 6PYA.

## D. Training

All experiments are conducted on 8 NVIDIA RTX 4090 GPUs with distributed data parallelism.

**Batching.** We employ a three-level batching strategy. First, each GPU processes one independent trajectory per training step. Second, for each trajectory we sample four subsequences (with random start indices and fixed stride) and compute the loss over all four in parallel. Third, for each target frame in a subsequence we denoise 12 independent noise samples (diffusion batch size=12) to stabilize the diffusion objective.

**Optimization.** We use the Adam optimizer with a learning rate of  $5 \times 10^{-4}$  and train for 40k steps.

**Data sampling.** During training we crop each system to a fixed size of 256 tokens. For mdCATH we take a contiguous crop of 256 residues; for MISATO we apply a spatial interface crop that includes the ligand and its surrounding protein residues. The maximum subsequence length is set to 20 for mdCATH and 10 for MISATO, corresponding to the different temporal scales of the two datasets.

**Loss weighting.** The training objective is a weighted sum of the reconstruction loss  $\mathcal{L}_{\text{recon}}$  and the latent fidelity loss  $\mathcal{L}_{\text{disto}}$  (defined in Section 3.4). We set  $\lambda_{\text{recon}} = 4.0$  and  $\lambda_{\text{disto}} = 0.03$ . The reconstruction loss also includes an atom-type weight  $w_{\text{entity}}(i)$ , set to 11.0 for ligand atoms and 1.0 for protein atoms. We use  $\sigma_{\text{data}} = 16$  following AlphaFold 3 (Abramson et al., 2024).

## E. Evaluation Metrics

### E.1. mdCATH

Following AlphaFlow (Jing et al., 2024a), we first evaluate the generated ensembles from three aspects: predicting flexibility, distributional accuracy, and ensemble observables. For each protein, the generated trajectory is compared against all replicas of the corresponding MD simulations.

**Predicting flexibility.** We assess the ability of a model to reproduce the dynamic fluctuations observed in MD simulations using three correlation-based metrics:

---

**Algorithm 5** ATMOS Inference

---

```

1: Input: Initial conformation  $\mathbf{x}_1$ , the chemical context  $\mathbf{a}$ .
2: Output: Generated trajectory  $\mathbf{X} = (\mathbf{x}_1, \mathbf{x}_2, \dots, \mathbf{x}_T) \in \mathcal{R}^{T \times N \times 3}$ .
3: Predefined: Number of keyframes  $M$ , upsampling factor  $u$ , coarse time step  $\Delta t^{\text{kf}} = u\Delta t$ .
4:  $\mathbf{s}_0, \mathbf{z}_0 \leftarrow \mathbf{e}_\theta(\mathbf{a})$  # Initialize latent state
5: keyframes  $\leftarrow [\mathbf{x}_1]$ 
6:
7: # Coarse-scale keyframe generation
8: for  $k \leftarrow 1$  to  $M - 1$  do
9:    $(\mathbf{v}^s, \mathbf{v}^z) \leftarrow \mathcal{E}_\theta(\text{keyframes}[-1], \mathbf{a})$  # Encode current frame
10:   $(\mathbf{s}_k, \mathbf{z}_k) \leftarrow \mathcal{T}_\theta(\mathbf{s}_{k-1}, \mathbf{z}_{k-1}, \mathbf{v}^s, \mathbf{v}^z, \Delta t^{\text{kf}})$  # Transition latent state
11:   $\mathbf{x}_k \leftarrow \text{DiffusionSampler}(\mathbf{s}_k, \mathbf{z}_k, \mathbf{a})$  # Sample next keyframe (Algorithm 4)
12:  keyframes.append( $\mathbf{x}_k$ )
13: end for
14:
15: # Fine-scale interpolation
16: trajectory  $\leftarrow []$ 
17: for  $m \leftarrow 0$  to  $M - 2$  do
18:   $\mathbf{s}_0, \mathbf{z}_0 \leftarrow \mathbf{e}_\theta(\mathbf{a})$ 
19:   $\mathbf{x}_{\text{start}}, \mathbf{x}_{\text{end}} \leftarrow \text{keyframes}[m], \text{keyframes}[m + 1]$ 
20:  trajectory.append( $\mathbf{x}_{\text{start}}$ )
21:   $(\mathbf{v}_{\text{end}}^s, \mathbf{v}_{\text{end}}^z) \leftarrow \mathcal{E}_\theta(\mathbf{x}_{\text{end}}, \mathbf{a})$ 
22:  rem_times  $\leftarrow u\Delta t$ 
23:  for  $k \leftarrow 1$  to  $u - 1$  do
24:     $(\mathbf{v}^s, \mathbf{v}^z) \leftarrow \mathcal{E}_\theta(\text{trajectory}[-1], \mathbf{a})$  # Encode current frame
25:     $(\mathbf{s}_k, \mathbf{z}_k) \leftarrow \mathcal{T}_\theta(\mathbf{s}_{k-1}, \mathbf{z}_{k-1}, \mathbf{v}^s, \mathbf{v}^z, \Delta t, \mathbf{v}_{\text{end}}^s, \mathbf{v}_{\text{end}}^z, \text{rem\_times})$  # Transition latent state
26:     $\mathbf{x} \leftarrow \text{DiffusionSampler}(\mathbf{s}_k, \mathbf{z}_k, \mathbf{a})$  # Sample next keyframe (Algorithm 4)
27:    trajectory.append( $\mathbf{x}$ )
28:    rem_times  $\leftarrow \text{rem\_times} - \Delta t$ 
29:  end for
30: end for
31:  $\mathbf{X} \leftarrow \text{trajectory}$ 
32: Return  $\mathbf{X}$ 

```

---

- **Pairwise RMSD  $r$ :** For each protein, we compute the average  $C\alpha$ -RMSD between every pair of conformations in the ensemble, which serves as a scalar measure of overall flexibility. The Pearson correlation between these pairwise RMSD values and those of the reference MD ensemble is reported.
- **Global RMSF  $r$ :** We calculate the root-mean-square fluctuation (RMSF) of each residue (represented by its  $C\alpha$  atom) across the ensemble. All per-residue RMSF values from all test proteins are concatenated, and the Pearson correlation with the reference RMSF values is computed.
- **Per-target RMSF  $r$ :** For each individual protein, we compute the Pearson correlation between the predicted and reference per-residue RMSF vectors. The median of these per-protein correlations across the test set is reported.

**Distributional accuracy.** We assess the model’s ability to reproduce the correct distribution of atomic positions using four metrics based on the 2-Wasserstein distance ( $\mathcal{W}_2$ ):

- **Root mean  $\mathcal{W}_2$ -dist:** The root mean Wasserstein distance (RMWD) between ensembles is defined as:

$$\text{RMWD}(\mathcal{X}, \mathcal{Y}) = \sqrt{\frac{1}{N} \sum_{i=1}^N \mathcal{W}_2^2(\mathcal{N}[\mathcal{X}_i], \mathcal{N}[\mathcal{Y}_i])}, \quad (16)$$

where  $\mathcal{N}[\mathcal{X}_i]$  denotes a 3D Gaussian fitted to the positional distribution of the  $i$ -th atom in ensemble  $\mathcal{X}$ . We report the median value over the test set.

- **MD PCA  $\mathcal{W}_2$ -dist:** To assess the similarity of collective motions, we project the  $C\alpha$  atom positions of the generated ensemble onto the first two principal components (PCs) derived from the reference MD ensemble. The 2-Wasserstein distance (in Angstrom units of RMSD) between the projected distributions of the generated and reference ensembles in this 2D PCA space is computed and reported.
- **Joint PCA  $\mathcal{W}_2$ -dist:** We perform PCA on the combined set of  $C\alpha$  atom positions from the generated and reference conformations (equally weighted) to obtain a joint set of principal components. Both ensembles are then projected onto the first two joint PCs, and the 2-Wasserstein distance between their projected  $C\alpha$  distributions is computed.
- **% PC-sim > 0.5:** For each protein, we compute the unsigned cosine similarity between the top principal component (derived from  $C\alpha$  positions) of the generated ensemble and that of the reference MD ensemble. A value exceeding 0.5 indicates that the dominant collective motion is successfully captured. We report the percentage of test proteins for which this condition holds.

**Ensemble observables.** To evaluate whether the model captures biologically relevant contact dynamics, we compute two sets of inter-residue contacts and compare them to the reference MD ensemble:

- **Weak contacts  $J$ :** We identify pairs of  $C\alpha$  atoms that are in contact (distance  $\leq 8\text{\AA}$ ) in the crystal structure but dissociate (distance  $> 8\text{\AA}$ ) in more than 10% of the ensemble structures. The Jaccard similarity between the set of such weak contacts in the generated ensemble and that in the reference MD ensemble is reported.
- **Transient contacts  $J$ :** Conversely, we identify pairs of  $C\alpha$  atoms that are not in contact (distance  $> 8\text{\AA}$ ) in the crystal structure but associate (distance  $\leq 8\text{\AA}$ ) in more than 10% of the ensemble structures. The Jaccard similarity between the generated and reference sets of transient contacts is reported.

Additionally, following TEMPO (Xu et al., 2025b), we report the **t-RMSD Error**, a trajectory-level metric that quantifies a model’s ability to reproduce the magnitude of conformational change over time. This metric is computed by (1) calculating the RMSD of each frame to the initial frame, and (2) computing the RMSE between the resulting RMSD sequences of the predicted and ground-truth trajectories.

## E.2. MISATO

The MISATO dataset captures the coupled dynamics of protein–ligand complexes, with the ligand’s motion confined to the protein’s binding pocket. For evaluation, we crop the pocket–ligand region. The pocket is defined as all residues where any heavy atom lies within  $10\text{\AA}$  of any ligand heavy atom, following the threshold used in AlphaFold 3 (Abramson et al., 2024).

We assess four aspects: flexibility prediction (per-target RMSF Pearson correlation), distributional accuracy (root mean 2-Wasserstein distance), steric clashes, and trajectory accuracy (t-RMSD Error). Except for steric clashes, the definitions align with those in Section E.1, but extended to include all atoms (protein and ligand).

Steric clashes are reported as the average number of clashes per generated trajectory. For ligand-only evaluation, we count clashes between ligand heavy atoms. For whole-complex evaluation, we count clashes between protein heavy atoms and ligand heavy atoms. A clash is defined as two heavy atoms being closer than  $1.1\text{\AA}$  again following AlphaFold 3 (Abramson et al., 2024).